# Nonlinear chirped interferometry for frequency-shift measurement and $\chi(3)$ spectroscopy

E. Neradovskaia, B. Maingot, G. Chériaux, C. Claudet, N. Forget, Aurélie Jullien

APL Photonics

# Nonlinear chirped interferometry for frequency-shift measurement and $\chi^{(3)}$ spectroscopy

Cite as: APL Photonics **7**, 116103 (2022); https://doi.org/10.1063/5.0109265
Submitted: 12 July 2022 • Accepted: 18 October 2022 • Accepted Manuscript Online: 19 October 2022 • Published Online: 04 November 2022

**E. Neradovskaia, B. Maingot, G. Chériaux, et al.**

# Nonlinear chirped interferometry for frequency-shift measurement and $\chi^{(3)}$ spectroscopy

Cite as: APL Photon. 7, 116103 (2022); doi: 10.1063/5.0109265
Submitted: 12 July 2022 • Accepted: 18 October 2022 •
Published Online: 4 November 2022



E. Neradovskaia,[1] B. Maingot,[1,2] G. Chériaux,[1] C. Claudet,[1] N. Forget,[2] and A. Jullien[1,a)]

## AFFILIATIONS

[1] Institut de Physique de Nice (INPHYNI), Université Côte d'Azur, CNRS, UMR 7010, 1361 route des Lucioles, 06560 Valbonne, France
[2] Fastlite, 165 route des Cistes, 06600 Antibes, France

[a)] **Author to whom correspondence should be addressed:** aurelie.jullien@inphyni.cnrs.fr

## ABSTRACT

Four-wave mixing processes are ubiquitous in ultrafast optics and the determination of the coefficients of the $\chi^{(3)}$ tensor is thus essential. We introduce a novel time-resolved ultrafast spectroscopic method to characterize the third-order nonlinearity on the femtosecond time-scale. This approach, coined as "nonlinear chirped interferometry," makes use of the variation of the optical group delay of a transmitted probe under the effect of an intense pump pulse in the nonlinear medium of interest. The observable is the spectral interference between the probe and a reference pulse sampled upstream and the metric is the transient swing of the probe group delay. We show that the detected signal is enhanced when the pulses are weakly chirped, and that, although interferometric, the method is intrinsically less sensitive to environmental phase fluctuations and drifts. By chirping adequately the reference pulse, the transient frequency shift of the probe pulses is also detected in the time domain and the detected nonlinear signal is enhanced. Nonlinear phase shifts as low as 10 mrad, corresponding to a frequency shift of 30 GHz, i.e., 0.01% of the carrier frequency, are detected without heterodyne detection or active phase-stabilization. The diagonal and/or non-diagonal terms of reference glasses ($SiO_2$) and crystals ($Al_2O_3$, $BaF_2$, $CaF_2$) are characterized. The method is finally applied to measure the soft vibration mode of $KTiOAsO_4$ (KTA).



## I. INTRODUCTION

The third-order susceptibility tensor $\chi^{(3)}$ governs both resonant and non-resonant nonlinear processes involving four-wave mixing.[1] The real part of the diagonal terms, responsible for the well-known optical Kerr-effect (OKE), plays a fundamental role in ultrafast optics where frequency-degenerated nonlinear processes are routinely used to modify, control, or characterize the spatial, spectral, and temporal properties of intense pulses. The non-diagonal terms of the tensor $\chi^{(3)}$ are also exploited in nonlinear processes such as cross-polarized wave generation[2] and are ubiquitous when intense waves of different polarizations are mixed in nonlinear media. This is, in particular, the case of most optical parametric amplifiers, which have become the backbone of third-generation femtosecond sources.[3] It is thus essential to determine the coefficients of the $\chi^{(3)}$ tensor of nonlinear media ranging from common optical glasses to exotic nonlinear birefringent crystals.

Experimental methods suitable to measure the real part of the $\chi^{(3)}$ tensor are numerous[1] and suffice it to say that OKE spectroscopy gathers time-resolved pump–probe techniques tracking the changes (polarization, frequency, spatial phase, or temporal phase) of a weak probe pulse under the effect of an intense pump pulse in the medium of interest, either with[4–8] or without[9,10] interferometric detection. Another related approach, two-beam coupling (2BC), relies on the mutual interaction between two noncollinear beams crossing in the medium.[11–15] Chirped spectral holography has been applied to Raman spectroscopy and involves strongly chirped probe pulse, so as to create a ps-scale temporal window and measure both instantaneous and delayed phase-shifts in a single acquisition.[16–18] All these methods have their own advantages and drawbacks, but

most of them require noise reduction to isolate the contribution of weak nonlinearities (averaging and/or modulation with heterodyne detection).

In this paper, we report a novel time-resolved ultrafast transient spectroscopy method to characterize third-order nonlinearity on the femtosecond time-scale. We coin this method as "nonlinear chirped interferometry."

The approach consists of measuring the variations of the first derivative of the nonlinear temporal phase, i.e., the optical group delay, rather than the phase changes, induced on a probe pulse by an intense pulse in a non-linear medium. We demonstrate that, under certain small chirp conditions, two distinct physical effects, spectral and temporal shifts, add up and that monitoring the optical group delay, via spectral interferometry, gives access to the nonlinear phase value and, therefore, to the nonlinear tensor terms of the medium of interest. We show, both theoretically and experimentally, that the method is

(i) interferometric, but by design, less sensitive to environmental phase fluctuations and drifts: no active stabilization or shielding of the interferometer is required, even for meter-scale interferometer,
(ii) sensitive: 10 mrad nonlinear phase-shifts can be detected without heterodyne detection,
(iii) selective: self-focusing although visible on the experimental data does not affect the measurement,
(iv) polarization sensitive: non-diagonal terms of the $\chi^{(3)}$ tensor can be independently measured, and
(v) temporally-resolved: both instantaneous and delayed nonlinear processes can be investigated.

Features (iv) and (v) are common to non-collinear pump–probe spectroscopy setups. The paper is organized as follows. The theoretical line-out of nonlinear chirped interferometry is described in Sec. II. The experimental setup and nonlinear materials are then described in Sec. III. Section IV presents measurement results: validation of the technique with known isotropic and $\chi^{(3)}$-anisotropic materials, followed by soft vibration mode measurement in an anisotropic crystal (KTA).

## II. PRINCIPLE

The setup is essentially a frequency-degenerated pump–probe experiment with an interferometric detection. As justified below, the probe optical group delay as a function of pump–probe delay is monitored, rather than the phase.

An illustration is available in Fig. 1(a). A strong pump beam ($P$) and a weak probe beam (Pr), of identical carrier frequency $\omega_0$, are weakly focused and cross in a thin optical sample. A small angle ($\simeq 1$) is introduced between the two beams to allow a spatial separation before/after the sample and a delay line controls the relative group delay between the two pulses ($\tau_{\mathrm{PPr}}$). Through cross-phase modulation (XPM), the probe pulse undergoes a transient nonlinear phase shift $\varphi_{\mathrm{NL}}(t)$. The temporal dependence of $\varphi_{\mathrm{NL}}$ causes a shift of the probe's instantaneous carrier frequency, $\pm\Omega$ [Fig. 1(b)]: a down-shift (shift toward the "red") on the rising edge of the pump pulse and an up-shift (shift toward the "blue") on the trailing edge of the pump pulse (for a medium characterized by a positive nonlinear index $n_2 > 0$).[19] $\Omega$ is proportional to the nonlinear phase and, thus, to the involved $\chi^{(3)}$ term.[19] In nonlinear spectroscopy, $\varphi_{NL}$ can be extracted from the transient variation of $\Omega$, although this frequency shift is usually too small to be measured with precision[20] and/or might be entangled with spectral distortions induced by other effects such as self-phase modulation. We assume in the following that this frequency shift, noted $\Omega = \Omega(\tau_{PPr})$, is small compared to the optical bandwidth $\Delta\omega$ such that $|\Omega| \ll \Delta\omega$.

Let $E_{\mathrm{P}}(\omega)$, $E_{\mathrm{R}}(\omega)$, and $E_{\mathrm{Pr}}(\omega)$ be the complex spectral amplitudes of, respectively, the pump, reference, and probe pulses. Their respective spectral phases are $\varphi_{\mathrm{P}}(\omega)$, $\varphi_{\mathrm{R}}(\omega)$, and $\varphi_{\mathrm{Pr}}(\omega)$ with the convention $E_k(\omega) = |E_k(\omega)|\exp[-i\varphi_k(\omega)]$, where $k$ is the wave label. Spectral phases are hereafter assumed as purely quadratic, with chirp coefficients, respectively, labeled $\varphi_k^{(2)}$. The spectral phases thus are

$$\varphi_k(\omega) = \varphi_k(\omega_0) + \tau_k(\omega_0)(\omega - \omega_0) + \varphi_k^{(2)}(\omega - \omega_0)^2/2, \quad (1)$$

where $\tau_k = \tau_k(\omega_0)$ stands for the group delay.

The coupling between the pump and probe beams is treated elsewhere and can be described by the following propagation equation for the probe field[14] in the limit of a purely electronic nonlinearity,

$$c\frac{\partial E_{\mathrm{Pr}}}{\partial z} + (n_{g,0} + 4\gamma I_{\mathrm{P}})\frac{\partial E_{\mathrm{Pr}}}{\partial t} = 2i\omega_0\gamma I_{\mathrm{P}}E_{\mathrm{Pr}} - 4\gamma\frac{\partial I_{\mathrm{P}}}{\partial t}E_{\mathrm{Pr}}, \quad (2)$$

where $I_{\mathrm{P}}$ is the time-dependent pump intensity, $n_{g,0}$ is the group index at $\omega_0$, and $\gamma$ is the nonlinear coupling coefficient. This expression holds as long as the input polarization states of the pump and probe beams are either parallel or perpendicular with respect to each other. The general expression of $\gamma$ is rather complex and depends on the polarization states of the pump and probe pulses as well as on the crystallographic orientation and symmetry of the sample. For an isotropic medium, far away from any resonance, the expressions of $\gamma$ in SI units, for, respectively, parallel and perpendicular polarizations, are

$$\gamma_{\parallel} = \frac{3}{4\varepsilon_0 n_0^2 c}\chi^{(3)}_{xxxx} = n_2, \quad (3)$$

$$\gamma_{\perp} = \frac{1}{4\varepsilon_0 n_0^2 c}\chi^{(3)}_{yyyy}. \quad (4)$$

The propagation Eq. (2) assumes slowly varying envelopes and neglects temporal dispersion, which is compatible with the thin medium assumption and/or narrowband pulses, as considered here. The effect of the pump field is three-fold: the group index is increased by $4\gamma I_{\mathrm{P}}$ [the left member of Eq. (2)], and two nonlinear source terms contribute to the propagation [the right member of Eq. (2)]. The first source term corresponds to XPM and is responsible for the frequency shift $\Omega$, while the second term induces gain and loss via an energy transfer between the two beams (2BC). The interplay between these three effects is rather complex but, to simplify, the change in wave velocity can be neglected while the XPM and 2BC may significantly reshape the transmitted probe pulse in both the spectral and time domains. As a general result, the optical group delay of the transmitted probe pulse $\tau_{\mathrm{Pr}}$ is altered when the pump and probe pulses overlap. For the sake of clarity, the probe group delays with and without the pump beam are, respectively, noted as $\tau_{\mathrm{Pr}}$ and $\tau^0_{\mathrm{Pr}}$.

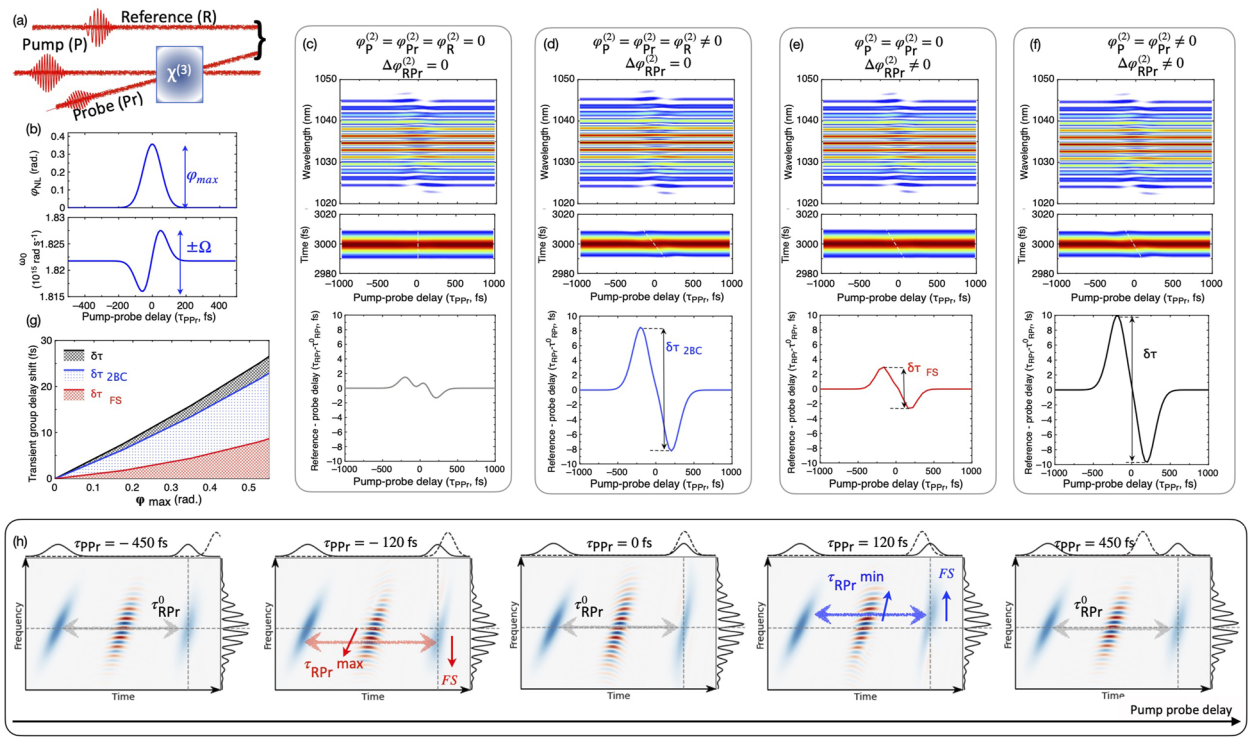


**FIG. 1.** (a) Principle of nonlinear chirped interferometry. (b)–(g) Numerical illustration for the numerical values indicated in the text. (b) Nonlinear XPM phase and shift of the carrier frequency of the transmitted probe pulse as a function of the pump–probe delay $\tau_{PPr}$. Top row of [(c)–(f)]: computed spectral interference $S(\omega)$ between the reference and the transmitted probe as a function of $\tau_{PPr}$. Middle row of [(c)–(f)]: modulus of the Fourier transform $|\hat{S}_{AC}(t-\tau^0_{RPr})|$ as a function of $\tau_{PPr}$. Bottom row of [(c)–(f)]: group delay shift of the transmitted probe $\tau_{RPr}-\tau^0_{RPr}$ as a function of $\tau_{PPr}$. The four columns correspond to the following cases: all three pulses are unchirped (c), all pulses are chirped by the same amount (d), only reference pulse is chirped (e), and all pulses are chirped with an additional chirp on the reference pulse (f). (g) Amplitude of the transient shift ($\delta\tau$) of the probe group delay as a function of the XPM nonlinear phase for the three cases [(d) blue line; (e) red line; (f) black line]. (h) Wigner–Ville distribution of the probe-reference electric fields for five different pump–probe delays $\tau_{PPr}$. For each sub-plot, the reference pulse is on the left and the (delayed) probe pulse is on the right. Both pulses are chirped and exhibit a time-dependent instantaneous frequency. The two pulses are chirped differently, and the slopes of the individual representations differ. In between the two pulses appears the interferometric component. Upper plot: integration of the distribution along the frequency coordinate (temporal intensity, solid line) compared to the cross-section of the pump pulse (dotted line). Right plot: integration of the distribution along the time coordinate [interference spectrum $S(\omega)$]. The large arrow indicates the reference–probe group delay $\tau_{RPr}$. For $\tau_{PPr}=\pm450$ fs (i.e., no temporal overlap between the pump and probe), $\tau_{RPr}=\tau^0_{RPr}$. For $\tau_{PPr}\lesssim 0$, the nonlinear phase induces a red shift of the transmitted probe (red arrow), which increases $\tau_{RPr}$. Symmetrically, for $\tau_{PPr}\gtrsim 0$, a blue shift decreases $\tau_{RPr}$. For $\tau_{PPr}=0$, there is no spectral shift and $\tau_{RPr}=\tau^0_{RPr}$. For all the sub-plots, 2BC stands for two-beam coupling and FS for frequency-shift.

As $\tau_{Pr}-\tau^0_{Pr}$ cannot be measured directly, the transmitted probe pulse is recombined with a reference pulse (in this case, a replica selected upstream) and the relative group delay $\tau_{RPr}=\tau_R-\tau_{Pr}$ between the reference and probe is measured instead. We note $\tau^0_{RPr}=\tau_R-\tau^0_{Pr}$ so that $\tau_{Pr}-\tau^0_{Pr}=\tau_{RPr}-\tau^0_{RPr}$. The relative delay $\tau^0_{RPr}$, which is kept constant during the experiment, is chosen adequately so as to be able to resolve the phase difference between the probe and reference pulses by spectral interferometry: $\Delta\omega \gg 1/|\tau^0_{RPr}| > \delta\omega_{sp}$, where $\delta\omega_{sp}$ is the spectral resolution of the spectrometer. The spectral interference pattern between the transmitted probe and the reference is

$$S(\omega)=|E_R(\omega)|^2+|E_{Pr}(\omega)|^2+2\mathrm{Re}\left\{E_R(\omega)E^*_{Pr}(\omega)\,e^{i\omega\tau_{RPr}}\right\}. \quad (5)$$

$S(\omega)$ contains one non-oscillating term (DC term) and two conjugate oscillating terms (AC terms), the Fourier-transform of which is

$$\hat{S}_{AC}(t-\tau_0)=\int E_R(\omega)E^*_{Pr}(\omega)\,e^{i\omega t}d\omega. \quad (6)$$

If $E_{Pr}(\omega)=E_R(\omega)$ (i.e., in the case without the pump wave), then $\hat{S}_{AC}(t-\tau^0_{RPr})$ is equal to the Fourier-transform of $|E_R(\omega)|^2$, and the AC terms are centered at $t=\pm\tau^0_{RPr}$ and well separated from the DC term at $t=0$. To anticipate on the following paragraphs, four-wave mixing introduces additional contributions to the optical group delay of the probe pulse and tends to shift the location of the AC terms from $\pm\tau^0_{RPr}$ to $\pm\tau_{RPr}$ (our observable). As shown below, this definition actually aggregates two distinct physical effects.

A numerical resolution of Eq. (2), described in the supplementary material, is proposed for a pump pulse duration of 180 fs FWHM, $I_P=300$ GW/cm$^2$, and a crystal of 1 mm length characterized by a nonlinear index $\gamma=n_2=2.810^{-16}$ cm$^2$/W. The corresponding nonlinear XPM phase is ≃300 mrad. Pump and

probe pulses are equally chirped, with a chirp coefficient of either $\varphi_P^{(2)} = \varphi_{Pr}^{(2)} = 0$ fs$^2$ or $\varphi_P^{(2)} = \varphi_{Pr}^{(2)} = +5000$ fs$^2$. The latter corresponds to a minor change in the pump pulse duration (195 fs). The reference pulse has a chirp coefficient of $\varphi_R^{(2)} = \varphi_{Pr}^{(2)} + \Delta\varphi_{RPr}^{(2)}$, with either $\Delta\varphi_{RPr}^{(2)} = 0$ fs$^2$ or $\Delta\varphi_{RPr}^{(2)} = +2000$ fs$^2$. The initial group delay between the probe and the reference pulses is $\tau_{Pr}^0 = 3$ ps. As our model is unidirectional, spatial effects such as Kerr lens and self-diffraction are not simulated.

We first consider the case $\varphi_P^{(2)} = \varphi_R^{(2)} = \varphi_{Pr}^{(2)} = 0$ fs$^2$, i.e., all involved pulses are limited by Fourier transform. The spectral interferogram as a function of pump–probe delay, $\tau_{PPr} = \tau_P - \tau_{Pr}^0$, is plotted in Fig. 1(c). The transient frequency shift $\Omega$ appears for $\Delta\Omega\tau_{PPr} \lesssim 1$, when the pump and probe pulses temporally overlap. For each pump–probe delay, the discrete Fourier transform of the spectral interferogram is computed. The relative group delay between the reference and probe pulses ($\tau_{RPr}$) is then the center of mass of the AC peak $|\hat{S}_{AC}(t - \tau_{RPr}^0)|$, retrieved by fitting the peak with a Gaussian function. As shown in Fig. 1(c), $\tau_{RPr} - \tau_{RPr}^0$ varies with the pump–probe delay $\tau_{PPr}$. When none of the three pulses are chirped, weak variations are observed, indicating that, to the first order, the optical group delay of the transmitted probe pulse is constant despite the spectral/temporal reshaping effects.

We then consider $\varphi_P^{(2)} = \varphi_R^{(2)} = \varphi_{Pr}^{(2)} = +5000$ fs$^2$, i.e., the three pulses are equally chirped. Because of this chirp, the instantaneous frequencies of the pump and probe pulses are detuned with respect to each other when $\tau_{PPr} \neq 0$. 2BC induces energy flows from one wave to the other during the nonlinear interaction. If the chirp coefficient is positive, the probe will gain energy for negative pump–probe delays and vice versa. As this energy transfer also scales with the pump intensity, the general effect is a reshaping of the temporal profile, which is indistinguishable from an additional optical group delay [Fig. 1(d)]. For negative pump–probe delays (resp. positive), the rear edge (resp. the leading edge) of the probe is strengthened, resulting in an overall increase (resp. decrease) of the group delay. As a result, $\tau_{RPr}$ exhibits a Z-shape, similar to the transient probe transmission reported for two-beam coupling.[11–13,15]

We now consider the case of unchirped pump and probe pulses $\varphi_P^{(2)} = \varphi_{Pr}^{(2)} = 0$ fs$^2$ with a positively chirped reference pulse $\varphi_R^{(2)} = +2000$ fs$^2$ [Fig. 1(e)]. The reference pulse being chirped, the frequency-shift $\Omega$ is temporally encoded in the interferogram and (also) appears as a delay $\tau_{RPr}$. As plotted in Fig. 1(e), this effect produces a similar Z-shape behaviour, although less pronounced than in the former case—but scaling linearly with $\Delta\varphi_{RPr}^{(2)} = \varphi_R^{(2)} - \varphi_{Pr}^{(2)}$. To illustrate the principle of spectral encoding, we present in Fig. 1 the Wigner–Ville distributions of the transmitted probe and of the delayed and chirped reference pulse. The relative chirp $\Delta\varphi_{RPr}^{(2)}$ makes the time–frequency slope different for each pulse, which is sufficient to encode a spectral shift as a temporal shift. As provided in the supplementary material, the linear relationship between the nonlinear frequency shift ($\Omega$) and the relative chirp between the probe and reference ($\Delta\varphi_{RPr}^{(2)}$) can be retrieved analytically from Eq. (6). We emphasize the fact that if $\Delta\varphi_{RPr}^{(2)} = 0$, this encoding cannot occur according to our model, in the small chirp configuration considered here.

We have evidenced here two phenomena: temporal reshaping (due to 2BC and triggered by $\varphi_P^{(2)} = \varphi_{Pr}^{(2)} \neq 0$) and temporal encoding of the nonlinear spectral shift (triggered by $\Delta\varphi_{RPr}^{(2)} \neq 0$). Although the differences between the spectrograms in Fig. 1 are not visible to the naked eye, the Fourier analysis shows that both mechanisms result in similar transient shifts of $\tau_{RPr}$, over the same temporal scale (the correlation width of the pump pulse), and with similar amplitudes (a few fs). With the right chirp parameters, these two contributions may add up and increase significantly the global signal-to-noise ratio of the measurement, as shown in Fig. 1(f). The delay swing $\delta\tau = \max(\tau_{RPr}) - \min(\tau_{RPr})$ is then our metric that evolves linearly with the nonlinear phase amount, as plotted in Fig. 1(g). As will be demonstrated experimentally in Sec. IV, measuring $\tau_{RPr}$ instead of phase changes not only makes the detection less sensitive to phase fluctuations but also gives additional means to enhance the sensitivity and specificity [Fig. 1(g)] of the detection, without resorting to heterodyne detection.

## III. EXPERIMENTAL METHODS

In the present experiments, a Pharos laser system (PH1-SP-1mJ, Light Conversion) delivers 180 fs FTL pulses, with a central wavelength of 1034 nm, a repetition rate of 10 kHz, and pulse energy up to 500 μJ. The laser chirp can be tuned by adjusting the compressor. Each pulse is split into three separated pulses: an excitation pump pulse, a probe pulse (≃20% of the pump energy), and a reference pulse selected before the nonlinear stage (Fig. 2). The pump and probe pulses are focused (f = 1.5 m) and overlap in the focal plane under a small angle (<1°) with a pump beam size of about 550 μm. The pump–probe delay ($\tau_{PPr}$) is controlled with a delay stage equipped by a motorized actuator with K-Cube controller (models Z825B and KDC101, Thorlabs). After the interaction, the probe is selected and recombined with the reference pulse. The nominal group delay between the reference and the probe pulses ($\tau_{RPr}^0$) is set to 3.5 ± 0.15 ps for all measurements. The interferometer extends over about 1–2 m. As shown in Sec. II, the chirp of all involved pulses has to be controlled independently. The laser compressor tunes the pump, probe, and reference chirp. Furthermore, the reference pulse can experience an additional chirp through the addition of various bulk plates: SF11 (20 mm, 2500 fs$^2$), $CaCO_3$(10 mm, 430 fs$^2$),[21] and $Al_2O_3$ (5 mm, 156 fs$^2$).[22] The resulting interference pattern is collected by a spectrometer (Avantes, spectral resolution 0.07 nm) for each step of the optical delay stage in the pump arm. The polarization and energy of each pulse are controlled by half-wave plates and thin-film polarizers (TFP). The different components of the $\chi^{(3)}$ tensor can then be measured by changing the polarization state of the three pulses.

The detailed procedure for data acquisition and analysis can be found in the supplementary material. To summarize, for each acquisition scan, $\tau_{PPr}$ is scanned (single scan) from −2.6 to 2.6 ps with temporal steps of 13 fs (400 spectra per scan). The integration time of the spectrometer is 1 ms (total acquisition time >1 mn, limited by the delay stage). The probe–reference delay and relative chirp are measured before each acquisition, out of pump–probe temporal overlap. $\tau_{RPr}$ is computed by fitting the modulus of the AC peak with a Gaussian function after discrete Fourier transform. The relative

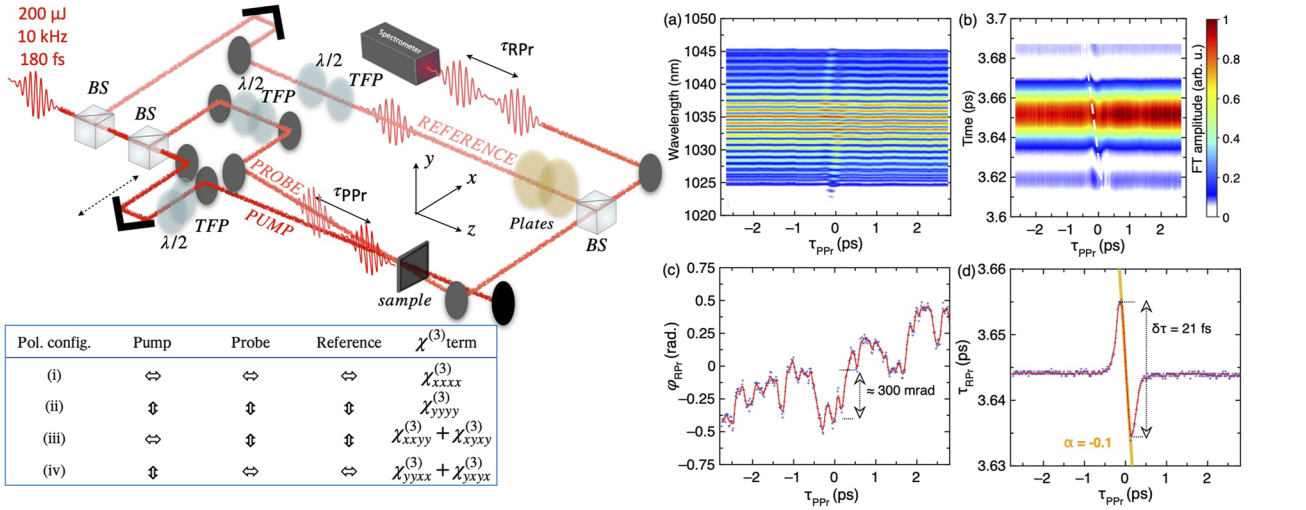


| Pol. config. | Pump | Probe | Reference | $\chi^{(3)}$term |
|---|---|---|---|---|
| (i) | ⇔ | ⇔ | ⇔ | $\chi^{(3)}_{xxxx}$ |
| (ii) | ⇕ | ⇕ | ⇕ | $\chi^{(3)}_{yyyy}$ |
| (iii) | ⇔ | ⇕ | ⇕ | $\chi^{(3)}_{xxyy}+\chi^{(3)}_{xyxy}$ |
| (iv) | ⇕ | ⇔ | ⇔ | $\chi^{(3)}_{yyxx}+\chi^{(3)}_{yxyx}$ |

**FIG. 2.** Optical setup. The laser source (Pharos SP, Light Conversion) is split into three beams (pump, probe, and reference). BS: beam splitter. TFP: thin film polarizer. $\lambda/2$: half-wave plates. Pump and probe beams are focused ($f$ = 1.5 m, not shown) on the nonlinear sample, positioned on a three-axis translation stage. Optional glass plates are inserted in the reference beam path. The table summarizes the polarization configurations and measured components of the $\chi^{(3)}$ tensor. (a)–(d) Typical experimental data for the 1 mm-thick sapphire. The nonlinear phase-shift accumulated by the probe is estimated to be 300 mrad and the normalized frequency-shift is $\Omega/\omega_0 \simeq 10^{-3}$. (a) Interferogram of the probe and reference pulses as a function of pump–probe delay. (b) AC peak of the Fourier transform of the interferograms. The white dashed line highlights the transient swing of the AC peak. (c) Relative phase between reference and probe pulses ($\varphi_{\mathrm{RPr}}$) as a function of pump–probe delay. (d) $\tau_{\mathrm{RPr}}$ as a function of pump–probe delay. For sub-plots [(c) and (d)]: raw data (blue), moving average (red), and linear fit (orange).

phase between the probe and reference pulses was also retrieved by Fourier filtering, so as to compare our analysis with usual nonlinear phase measurements.

The method was validated against a set of isotropic materials for which the nonlinear refractive indices are well known: fused silica [1 mm, $(2.2 \pm 0.3) \times 10^{-16}$ cm$^2$/W at 1030 nm],[23] barium fluoride [0.5 mm, $(2.2 \pm 0.2) \times 10^{-16}$ cm$^2$/W at 1064 nm],[24] sapphire [1 mm, $(2.8 \pm 0.7) \times 10^{-16}$ cm$^2$/W at 1030 nm],[25] and calcium fluoride [1 mm, $(1.2 \pm 0.3) \times 10^{-16}$ cm$^2$/W at 1030 nm].[23] All plates are uncoated. In order to check the validity of various polarization configurations, we also characterized a barium fluoride crystal, with a holographic [011] crystallographic orientation, which is known to present an anisotropy of its third-order nonlinearity, $\sigma$, defined as follows:[26,27]

$$\sigma = \frac{\chi^3_{xxxx} - 2\chi^3_{xyyx} - \chi^3_{xxyy}}{\chi^3_{xxxx}}. \tag{7}$$

## IV. RESULTS

The method is validated in three steps. We first compare the numerical model with experimental data and measure the swing amplitude of $\tau_{\mathrm{RPr}} - \tau^0_{\mathrm{RPr}}$ with respect to the relative chirps and nonlinear phase. We then measure the diagonal third-order tensor coefficient of a set of well-known isotropic samples. Next, we vary the polarization states of the pump and probe beams, characterize the nonlinear anisotropy of barium fluoride, and compare the measured coefficients with the reported values. Finally, we investigate the instantaneous and delayed nonlinear properties of potassium titanyl arsenate (KTA) crystals.

### A. Comparison with the numerical model

All polarization directions are first set to horizontal. The pump energy is 40 µJ, which corresponds to a pump peak intensity estimated to 300 GW/cm$^2$ on the sample. The measured chirp coefficients are $\varphi^{(2)}_{\mathrm{P}} = \varphi^{(2)}_{\mathrm{Pr}} = (+5000 \pm 500)$ fs$^2$ and $\Delta\varphi^{(2)}_{\mathrm{RPr}} = (+2000 \pm 100)$ fs$^2$. These GDD values are quite low and pulses durations are then, respectively, 195, 195, and 210 fs, for the pump, probe, and reference, respectively, as confirmed with Wizzler measurements. Figure 2 gathers typical experimental results acquired for a 1 mm c-cut sapphire crystal. As expected [Fig. 2(a)], in the vicinity of $\tau_{\mathrm{PPr}} = 0$, a red-shift is observed for $\tau_{\mathrm{PPr}} < 0$ while a blue-shift is observed for $\tau_{\mathrm{PPr}} > 0$. Self-focusing is visible on the experimental data as a transient signal decrease. It translates as a slight change in the Fourier transform amplitude but does not affect the measurement. A close-up of the Fourier transform near +3.5 ps is shown in Fig. 2(b). The transient shift of the peak position ($\tau_{\mathrm{RPr}}$) is clearly distinguishable. The latter, plotted in Fig. 2(d), shows the characteristic z-shape, in excellent agreement with Fig. 1. The delay swing $\delta\tau = \max(\tau_{\mathrm{RPr}}) - \min(\tau_{\mathrm{RPr}}) = 21$ fs is obtained for $\tau_{\mathrm{PPr}} = \pm 100$ fs with a linear dependence of the signal between these two extrema (a slope of $\simeq -0.1$). For the sake of comparison, Fig. 2(c) represents the relative phase between the reference and the transmitted probe pulses extracted from the spectrogram by Fourier filtering. This metric is the quantity usually measured to determine the value of the non-linear phase. However, in our experimental configuration (energetic pulses, meter-scale interferometer without any active stabilization), $\varphi_{\mathrm{NL}}$ can hardly be distinguished from the phase noise (fluctuations and drifts, rms phase noise about 100 mrad) added by the interferometer, as can be seen in Fig. 2(c). The comparison

between Figs. 2(c) and 2(d) helps in appreciating the improvement in signal-to-noise ratio of our method. Monitoring the group delay rather than the spectral phase is, indeed, less sensitive to phase fluctuations and makes it possible to measure a nonlinear signal at least an order of magnitude weaker.

Starting from this working configuration, we then characterize $\delta\tau$ as a function of (i) $\varphi_{P}^{(2)} = \varphi_{Pr}^{(2)}$ (controlled by the grating compressor), (ii) $\Delta\varphi_{RPr}^{(2)}$ (controlled by adding/removing bulk in the reference beam path), and (iii) pump energy—all other experimental parameters being kept constant. The acquired raw data are shown in Fig. 3. As explained in Sec. II, $\varphi_{P}^{(2)}$ mainly triggers 2BC, meanwhile $\Delta\varphi_{RPr}^{(2)}$ enables temporal encoding of the frequency shift. The numerical model reproduces well the variations of $\tau_{RPr}$ and $\Omega$ (normalized with respect to $\omega_0$) with the pump chirp [Fig. 3(a)]. The frequency-shift follows the parabolic evolution of pump intensity, with a maximum close to pulse compression. Conversely, $\delta\tau$ varies mostly linearly (V-shape) around a minimum, staggered from the compression. We can distinguish several trends, as labeled in Fig. 3(a). For moderate positive input chirp (1), the frequency-shift remains mostly constant (i.e., so is the nonlinear phase) while $\delta\tau$ exhibits a linear increase with the pump chirp value, emphasizing how the signal to noise ratio is enhanced by 2BC. This area then defines the efficient working conditions of our method and emphasizes the need of a chirped pump. For negative input chirp (2), a similar trend is observed, but with a reversed Z-shape, as shown in the raw data in Fig. 3(b). Reversing the sign of the chirp is, in fact, equivalent to modify the sign of the energy couplings between the pump and the probe and, thus, to reverse the signal. The minimum of the $\delta\tau$ V-shape (3) corresponds to a weak signal with an ill-defined shape [Fig. 3(b)]. The large offset from pulse compression is both predicted by the model and observed. It matches the reference–probe relative chirp, $-2000$ fs$^2$, and results from the compensation of the temporal and spectral contributions detailed before. The numerical fit agrees quite well with the experimental data, except for the large chirps (4). This discrepancy is attributed to higher orders of spectral phase (neglected in the model).

The increase in $\delta\tau$ with $\Delta\varphi_{RPr}^{(2)}$ is shown in Fig. 3(c). The pump energy is kept constant. For $\Delta\varphi_{RPr}^{(2)} \simeq 0$, there is no encoding of the spectral shift and $\delta\tau = 12$ fs corresponds to the 2BC contribution, in good agreement with the model. When $\Delta\varphi_{RPr}^{(2)}$ increases, the contribution from the spectral shift leads to a linear increase in $\delta\tau$. The colored area in Fig. 3(c) highlights the different contribution (2BC from the chirped pump in blue and frequency-shift from the probe-reference relative chirp in red). In the studied configuration, although 2BC is the strongest effect, $\Delta\varphi_{RPr}^{(2)}$ is an additional degree of freedom, easy to implement experimentally, particularly useful to increase $\delta\tau$ in order to detect a weak amount of nonlinear phase.

Finally, we characterize how $\delta\tau$ and $\Omega$ scale with the pump intensity by scanning the pump energy from 5 to 80 μJ. Figure 3(d) evidences the linear dependence of both $\delta\tau$ and $\Omega$ with the pump energy up to 50 μJ. This measurement also exemplifies that frequency shifts spanning over more than an order of magnitude (from 30 to 400 GHz, i.e., from 0.01% to 0.2% of the carrier frequency) can be detected in a single scan. The lowest measured phase-shift is about 10 mrad with single-shot detection, which is one order of magnitude

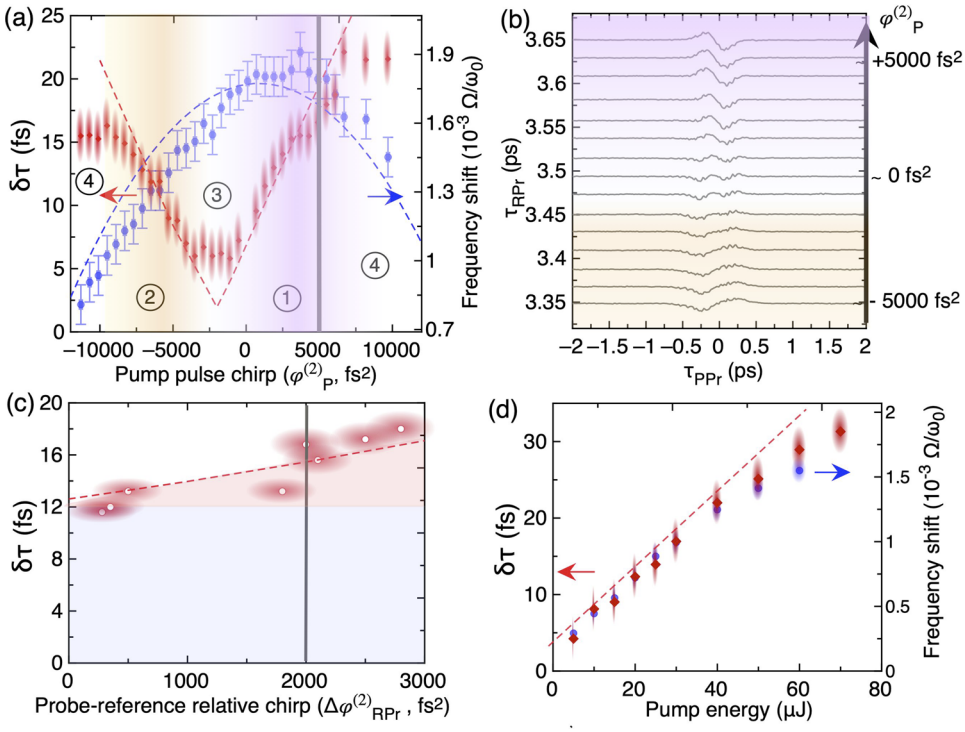


**FIG. 3.** Experimental data compared to the numerical 1D simulations. The clouds indicate the dispersion of the experimental data. (a) $\delta\tau$ (red) and normalized frequency shift ($\Omega/\omega_0$, blue) as a function of input chirp $\varphi_{P}^{(2)} = \varphi_{Pr}^{(2)}$, for $\Delta\varphi_{RPr}^{(2)} = (+2000 \pm 100)$ fs$^2$. The colored area and labels refer to different zones of interest (see the text). (b) $\tau_{RPr}$ as a function of $\tau_{PPr}$, for various $\varphi_{P}^{(2)}$ values, indicated on the right y-scale. The curves are artificially shifted for clarity. The colored area correspond to those in (a). (c) $\tau_{RPr}$ as a function of the chirp difference between the reference and pump/probe pulses, $\Delta\varphi_{RPr}^{(2)}$, with fixed input chirp $\varphi_{P}^{(2)} = (+5000 \pm 500)$ fs$^2$. The colored area refers to 2BC (blue) and frequency-shift (red) contributions. (d) $\delta\tau$ (red) and normalized frequency shift ($\Omega/\omega_0$, blue) as a function of the pump energy for the chirp values indicated by the gray lines in plots (a) and (c).

**TABLE I.** $\chi^{(3)}$ ratio between validation set plates, normalized to the fused silica nonlinear term hereafter labeled as $\chi_0$, and compared to the values found in the literature.[23–25] $\chi_0 = (2.0 \pm 0.2)10^{-22}$ m$^2$/V$^2$, as reported in Ref. 29.

| Sample | $\chi^{(3)}/\chi_0$ (this work) | $\chi^{(3)}_{lit}/\chi_0$ (literature) |
|---|---|---|
| $Al_2O_3$ | $(1.1 \pm 0.2)$ | $(1.3 \pm 0.3)$ |
| $BaF_2$ | $(1.0 \pm 0.1)$ | $(1.0 \pm 0.1)$ |
| $CaF_2$ | $(0.5 \pm 0.02)$ | $(0.6 \pm 0.1)$ |

**TABLE II.** Nonlinear anisotropy of $BaF_2$ with [011] crystallographic orientation.

| Polarization configuration | $\sigma$ (this work) | $\sigma$ (literature)[26] |
|---|---|---|
| (i), (ii) | $-1.32 \pm 0.1$ | $-1.15 \pm 0.1$ |
| (i), (iii) | $-1.42 \pm 0.1$ | $-1.15 \pm 0.1$ |

**TABLE III.** Nonlinear refractive index at 1 μm of KTA ($\times 10^{-20}$ m$^2$/W), for 180 fs pulses.

| Sample | $n_{2,slow}$ | $n_{2,fast}$ |
|---|---|---|
| KTA | $7.8 \pm 0.2$ | $6.5 \pm 0.2$ |

lower than the large-scale interferometric setups without averaging and/or heterodyne detection.[6,7,11]

To summarize this sub-section, (i) experimental data are found in very good agreement with the numerical model, (ii) the expected trends of the signal dependence on involved chirp parameters have been recovered, and (iii) suitable chirp values and pump energy ranges so as to monitor nonlinear phase changes have been identified.

## B. Application to isotropic and anisotropic crystals

Although the method can, in principle, provide the absolute value of the nonlinear index, experimental sources of error are numerous (actual peak intensity, uncertainties on chirps. . .) and, in this work, we characterize $\delta\tau$ relatively to a reference sample, hereafter fused silica. The experimental parameters are those shown in Fig. 2. Table I gathers the measured $\chi^{(3)}$ ratio between the samples to characterize ($Al_2O_3$, $BaF_2$, $CaF_2$) and fused silica ($\chi^{(3)}_0$). A good agreement with published data ($\chi^{(3)}_{lit}$) is found. It can be noted that the error interval is similar to or lower than the ones given in the literature.

The last step of this validation process consists of changing the set of polarizations to check the symmetry properties of the nonlinear tensor. Comparison between polarization configuration (i)–(iii), as defined in Fig. 2, enables us to verify the tensor symmetry for fused silica: $\chi^{(3)}_{0,xxxx} = \chi^{(3)}_{0,yyyy}$ and $\chi^{(3)}_{0,xxyy} = \chi^{(3)}_{0,yyxx} \simeq \chi^{(3)}_{0,xxxx}/3$. Then, $BaF_2$ with a holographic orientation was characterized. The

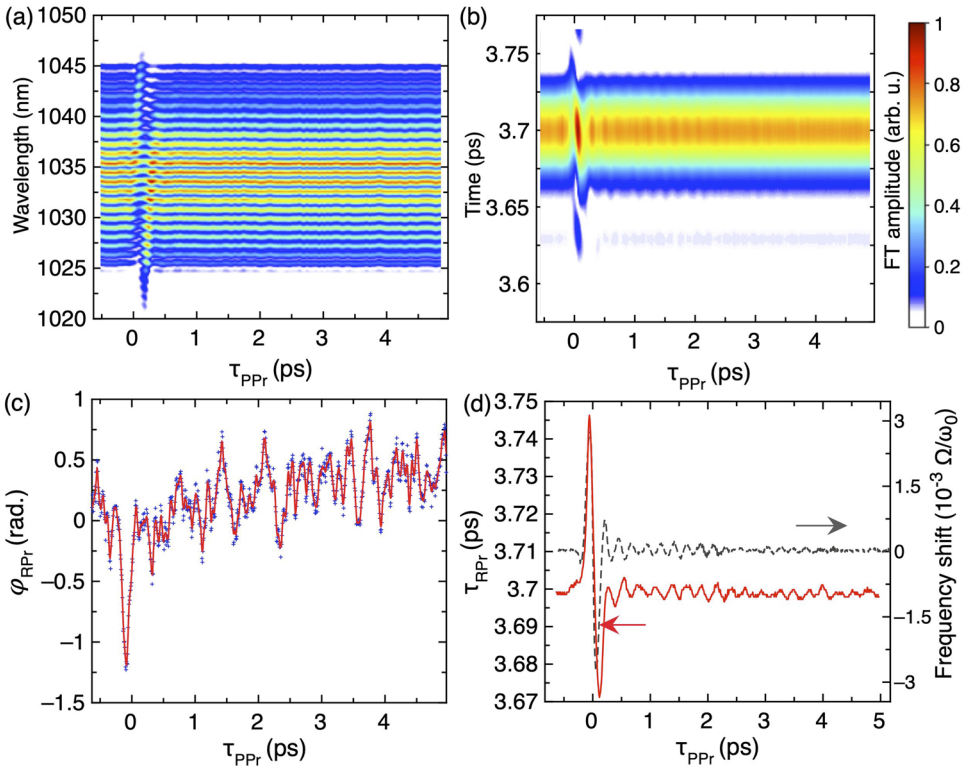


**FIG. 4.** Experimental data for the KTA crystal on a 6 ps scan range. (a) Interferogram of the probe and reference pulses as a function of pump–probe delay. (b) AC peak of the Fourier transform of the interferograms. (c) Relative phase between reference and probe pulses ($\varphi_{RPr}$) as a function of pump–probe delay. Raw data (blue), moving average (red). (d) $\tau_{RPr}$ (red) and normalized frequency shift (gray) as a function of pump–probe delay.

ratio between $\delta\tau$ obtained for two distinct polarization configurations leads to determination of the ratio between SPM and XPM $\chi^{(3)}$ terms and, thus, to the nonlinear anisotropy of $\chi^{(3)}$ [$\sigma$, Eq. (7)].[26–28] Our results are summarized in Table II, and once again, a good agreement between the values found in the literature is obtained.

Finally, we study the nonlinear properties of a Potassium Titanyl Arsenate (KTA) crystal along $\theta = 47^\circ$ and $\phi = 0^\circ$ (X–Z plane, thickness of 2 mm). The pump energy is reduced to 15 μJ, so as to keep the nonlinear phase within the linearity range indicated in Fig. 3(d). The polarization configurations are successively set to (i) and (ii), to measure the nonlinear indices of the fast and slow axes. Our results are gathered in Table III and found to be slightly lower than previous measurements reported using the Z-scan technique.[30]

Although outside the range of validity of the model developed above, a proof-of-principle measurement shows that delayed linear phenomena can also be investigated with our method. The temporal scanning range is then increased to +5 ps, so as to evidence the delayed nonlinear answer of KTA (fast axis). The results are shown in Fig. 4.

For this measurement, the pump energy is increased to 75 μJ to increase the signal-to-noise ratio at positive pump–probe delays. The group delay swing shows an asymmetry, followed by pseudo-periodic oscillations. This measurement evidences two main vibration modes, with respective wave numbers of 66 and 75 $cm^{-1}$, matching A1 vibrational frequencies of KTA, as reported in Ref. 31. In case of a delayed nonlinear response, the signal seems mainly originating from temporal transcription of the phonon-induced spectral shift, as shown in Fig. 4(d), where temporal and spectral oscillations perfectly match. This final measurement illustrates the potential application of our method to low-frequency Raman spectroscopy.[32]

## V. CONCLUSION

To conclude, we have introduced a novel time-resolved spectroscopic method to characterize the third-order nonlinearity on the femtosecond time-scale. This approach, coined as "nonlinear chirped interferometry," consists of monitoring the variations of the first derivative of the nonlinear temporal phase, i.e., the optical group delay, of a transmitted probe under the effect of a strong pump pulse, rather than the phase, via spectral interferometry between the probe and a reference pulse sampled upstream. We have shown that, under weak chirp conditions on the three involved pulses, the optical group delay transient changes originate from two different mechanisms, coherently added up: (i) 2BC triggers energy exchanges between chirped pump and probe pulses and induces temporal reshaping and (ii) the XPM frequency-shift undergone by the probe is encoded in time by adequately chirping the reference pulse. Due to a good agreement between experimental data and a 1D numerical model, we have been able to define the experimental working area of our method, in terms of chirp of involved pulses and nonlinear phase amount.

Thus, we have demonstrated that monitoring the optical group delay instead of phase makes the detection intrinsically less sensitive to phase fluctuations. No active stabilization is required, even for the meter-scale interferometer, as it was studied in this paper. The method provides additional means to enhance the sensitivity and specificity of the detection, without resorting to heterodyne detection. Nonlinear phase shifts as low as 10 mrad, corresponding to a frequency shift of 30 GHz, i.e., 0.01% of the carrier frequency, can thus be detected. The method is suited to perform non-resonant $\chi^{(3)}$ spectroscopy in isotropic or anisotropic nonlinear media, but also to survey resonant and delayed nonlinear processes. This original approach could be easily exported to the detection of spectral shifts driven by other linear or nonlinear processes, among them fluorescence, and Raman spectroscopy.

Finally, the sensitivity reported here could be pushed further by multiple scans acquisition, higher averaging, and extending the involved spectral bandwidths.

## SUPPLEMENTARY MATERIAL

In the supplementary material, details are provided about the numerical model used in this study and an analytical calculation is proposed to illustrate the encoding of the frequency-shift of the probe pulse as a group delay change, when recombining the shifted signal with a chirped delayed local oscillator (reference).

## ACKNOWLEDGMENTS

The authors acknowledge the financial support from the Agence Nationale de la Recherche France (Grant No. ANR-19-CE30-0006-01 UNLOC), the European Regional Development Fund (OPTIMAL), and from the European Union's Horizon 2020 research and innovation program under the Marie Skłodowska-Curie Grant Agreement No. 860553.

## AUTHOR DECLARATIONS

### Conflict of Interest

The authors have no conflicts to disclose.

### Author Contributions

**E. Neradovskaia**: Data curation (equal); Formal analysis (equal); Investigation (equal); Methodology (equal); Software (equal); Writing – original draft (equal). **B. Maingot**: Data curation (equal); Formal analysis (equal); Investigation (equal); Methodology (equal); Software (equal). **G. Chériaux**: Funding acquisition (supporting); Investigation (supporting); Resources (supporting). **C. Claudet**: Investigation (supporting); Methodology (supporting); Resources (supporting). **N. Forget**: Formal analysis (equal); Investigation (equal); Methodology (equal); Validation (equal); Writing – original draft (equal); Writing – review & editing (equal). **A. Jullien**: Conceptualization (lead); Data curation (equal); Funding acquisition (lead); Investigation (equal); Methodology (equal); Project administration (lead); Supervision (lead); Validation (equal); Visualization (equal); Writing – original draft (equal); Writing – review & editing (lead).

## DATA AVAILABILITY

The data that support the findings of this study are available from the corresponding author upon reasonable request.

## REFERENCES


[1] R. L. Sutherland, *Handbook of Nonlinear Optics* (Marcel Dekker, 2003).

[2] A. Jullien, O. Albert, F. Burgy, G. Hamoniaux, J.-P. Rousseau, J.-P. Chambaret, F. Augé-Rochereau, G. Chériaux, J. Etchepare, N. Minkovski, and S. M. Saltiel, "$10^{-10}$ temporal contrast for femtosecond ultraintense lasers by cross-polarized wave generation," Opt. Lett. **30**, 920–922 (2005).

[3] H. Fattahi, H. G. Barros, M. Gorjan, T. Nubbemeyer, B. Alsaif, C. Y. Teisset, M. Schultze, S. Prinz, M. Haefner, M. Ueffing *et al.*, "Third-generation femtosecond technology," Optica **1**, 45–63 (2014).

[4] R. DeSalvo, A. A. Said, D. J. Hagan, E. W. Van Stryland, and M. Sheik-Bahae, "Infrared to ultraviolet measurements of two-photon absorption and $n_2$ in wide bandgap solids," IEEE J. Quantum Electron. **32**, 1324 (1996).

[5] C. Y. Chien, B. La Fontaine, A. Desparois, Z. Jiang, T. W. Johnston, J. C. Kieffer, H. Pépin, F. Vidal, and H. P. Mercure, "Single-shot chirped-pulse spectral interferometry used to measure the femtosecond ionization dynamics of air," Opt. Lett. **25**, 578–580 (2000).

[6] Y.-H. Chen, S. Varma, I. Alexeev, and H. Milchberg, "Measurement of transient nonlinear refractive index in gases using xenon supercontinuum single-shot spectral interferometry," Opt. Express **15**, 7458–7467 (2007).

[7] Á. Börzsönyi, Z. Heiner, A. P. Kovács, M. P. Kalashnikov, and K. Osvay, "Measurement of pressure dependent nonlinear refractive index of inert gases," Opt. Express **18**, 25847–25854 (2010).

[8] J. Burgin, C. Guillon, and P. Langot, "Femtosecond investigation of the noninstantaneous third-order nonlinear suceptibility in liquids and glasses," Appl. Phys. Lett. **87**, 211916 (2005).

[9] S. P. Le Blanc, E. W. Gaul, N. H. Matlis, A. Rundquist, and M. C. Downer, "Single-shot measurement of temporal phase shifts by frequency-domain holography," Opt. Lett. **25**, 764–766 (2000).

[10] R. Thurston, M. M. Brister, A. Belkacem, T. Weber, N. Shivaram, and D. S. Slaughter, "Time-resolved ultrafast transient polarization spectroscopy to investigate nonlinear processes and dynamics in electronically excited molecules on the femtosecond time scale," Rev. Sci. Instrum. **91**, 053101 (2020).

[11] I. Kang, T. Krauss, and F. Wise, "Sensitive measurement of nonlinear refraction and two-photon absorption by spectrally resolved two-beam coupling," Opt. Lett. **22**, 1077–1079 (1997).

[12] S. Smolorz and F. Wise, "Femtosecond two-beam coupling energy transfer from Raman and electronic nonlinearities," J. Opt. Soc. Am. B **17**, 1636–1644 (2000).

[13] S. Smolorz, F. Wise, and N. F. Borrelli, "Measurement of the nonlinear optical response of optical fiber materials by use of spectrally resolved two-beam coupling," Opt. Lett. **24**, 1103 (1999).

[14] J. K. Wahlstrand, J. H. Odhner, E. T. McCole, Y.-H. Cheng, J. P. Palestro, R. J. Levis, and H. M. Milchberg, "Effect of two-beam coupling in strong-field optical pump-probe experiments," Phys. Rev. A **87**, 053801 (2013).

[15] G. N. Patwardhan, J. S. Ginsberg, C. Y. Chen, M. M. Jadidi, and A. L. Gaeta, "Nonlinear refractive index of solids in mid-infrared," Opt. Lett. **46**, 1824–1827 (2021).

[16] J. W. Wilson, P. Schlup, and R. Bartels, "Phase measurement of coherent Raman vibrational spectroscopy with chirped spectral holography," Opt. Lett. **33**, 2116–2118 (2008).

[17] K. Hartinger and R. A. Bartels, "Single-shot measurement of ultrafast time-varying phase modulation induced by femtosecond laser pulses with arbitrary polarization," Appl. Phys. Lett. **92**, 021126 (2008).

[18] P. Schlup, J. W. Wilson, and R. A. Bartels, "Sensitive and selective detection of low-frequency vibrational modes through a phase-shifting fourier transform spectroscopy," IEEE J. Quantum Electron. **45**, 777 (2009).

[19] R. W. Boyd, *Nonlinear Optics* (Academic Press, 1992).

[20] J.-F. Ripoche, G. Grillon, B. Prade, M. Franco, E. Nibbering, R. Lange, and A. Mysyrowicz, "Determination of the time dependence of $n_2$ in air," Opt. Commun. **135**, 310 (1997).

[21] G. Ghosh, "Dispersion-equation coefficients for the refractive index and birefringence of calcite and quartz crystals," Opt. Commun. **163**, 95–102 (1999).

[22] I. H. Malitson and M. J. Dodge, "Refractive index and birefringence of synthetic sapphire," J. Opt. Soc. Am. **62**, 1405 (1972).

[23] P. Kabaciński, T. M. Kardaś, Y. Stepanenko, and C. Radzewicz, "Nonlinear refractive index measurement by SPM-induced phase regression," Opt. Express **27**, 11018–11028 (2019).

[24] R. Adair, L. L. Chase, and S. A. Payne, "Nonlinear refractive index of optical crystals," Phys. Rev. B **39**, 3337–3350 (1989).

[25] A. Major, F. Yoshino, I. Nikolakakos, J. S. Aitchison, and P. W. E. Smith, "Dispersion of the nonlinear refractive index in sapphire," Opt. Lett. **29**, 602–604 (2004).

[26] N. Minkovski, G. I. Petrov, S. M. Saltiel, O. Albert, and J. Etchepare, "Nonlinear polarization rotation and orthogonal polarization generation experienced in a single-beam configuration," J. Opt. Soc. Am. B **21**, 1659–1664 (2004).

[27] L. Canova, S. Kourtev, N. Minkovski, A. Jullien, R. Lopez-Martens, O. Albert, and S. M. Saltiel, "Efficient generation of cross-polarized femtosecond pulses in cubic crystals with holographic cut orientation," Appl. Phys. Lett. **92**, 231102 (2008).

[28] S. Kourtev, N. Minkovski, L. Canova, A. Jullien, O. Albert, and S. M. Saltiel, "Improved nonlinear cross-polarized wave generation in cubic crystals by optimization of the crystal orientation," J. Opt. Soc. Am. B **26**, 1269–1275 (2009).

[29] U. Gobler and C. Bosshard, "Optical third-harmonic generation of fused silica in gas atmosphere: Absolute value of the third-order nonlinear optical susceptibility," Phys. Rev. B **61**, 10702 (2000).

[30] H. P. Li, C. H. Kam, Y. L. Lam, and W. Ji, "Femtosecond Z-scan measurements of nonlinear refraction in nonlinear optical crystals," Opt. Mater. **15**, 237–242 (2001).

[31] C. S. Tu, A. R. Guo, R. Tao, R. S. Katiyar, R. Guo, and A. S. Bhalla, "Temperature dependent Raman scattering in $KTiOPO_4$ and $KTiOAsO_4$ single crystals," J. Appl. Phys. **79**, 3235 (1996).

[32] D. R. Smith, J. J. Field, D. G. Winters, S. R. Domingue, F. Rininsland, D. J. Kane, J. W. Wilson, and R. A. Bartels, "Phase noise limited frequency shift impulsive Raman spectroscopy," APL Photonics **6**, 026107 (2021).